On the quantum dynamical treatment of surface vibrational modes for reactive scattering of H2 from Cu(111) at 925 K

Sah Mantu, K.; Naskar, K.; Adhikari, S.; Smits, B.; Meyer, J., Somers, M.F.

The Journal of Chemical Physics

RESEARCH ARTICLE | JULY 02 2024

On the quantum dynamical treatment of surface vibrational modes for reactive scattering of H_2 from Cu(111) at 925 K

Mantu Kumar Sah ; Koushik Naskar ; Satrajit Adhikari ; Bauke Smits ; Jörg Meyer ; Mark F. Somers

J. Chem. Phys. 161, 014306 (2024)
https://doi.org/10.1063/5.0217639

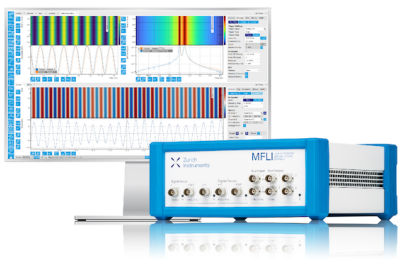

AIP Publishing

The Journal of Chemical Physics ARTICLE pubs.aip.org/aip/jcp

On the quantum dynamical treatment of surface vibrational modes for reactive scattering of H_2 from Cu(111) at 925 K

Cite as: J. Chem. Phys. 161, 014306 (2024); doi: 10.1063/5.0217639
Submitted: 6 May 2024 • Accepted: 13 June 2024 •
Published Online: 2 July 2024

Mantu Kumar Sah,[1] Koushik Naskar,[1] Satrajit Adhikari,[1,a)] Bauke Smits,[2] Jörg Meyer,[2] and Mark F. Somers[2]

AFFILIATIONS

[1] School of Chemical Sciences, Indian Association for the Cultivation of Science, Jadavpur, Kolkata 700032, India
[2] Leiden Institute of Chemistry, Gorlaeus Building, Leiden University, P.O. Box 9502, 2300 RA Leiden, The Netherlands

[a)] **Author to whom correspondence should be addressed:** pcsa@iacs.res.in

ABSTRACT

We construct the effective Hartree potential for H_2 on Cu(111) as introduced in our earlier work [Dutta *et al.*, J. Chem. Phys. **154**, 104103 (2021), and Dutta *et al.*, J. Chem. Phys. **157**, 194112 (2022)] starting from the same gas–metal interaction potential obtained for 0 K. Unlike in that work, we now explicitly account for surface expansion at 925 K and investigate different models to describe the surface vibrational modes: (i) a cluster model yielding harmonic normal modes at 0 K and (ii) slab models resulting in phonons at 0 and 925 K according to the quasi-harmonic approximation—all consistently calculated at the density functional theory level with the same exchange–correlation potential. While performing dynamical calculations for the $H_2(v = 0, j = 0)$–Cu(111) system employing Hartree potential constructed with 925 K phonons and surface temperature, (i) the calculated chemisorption probabilities are the highest compared to the other approaches over the energy domain and (ii) the threshold for the reaction probability is the lowest, in close agreement with the experiment. Although the survival probabilities ($v' = 0$) depict the expected trend (lower in magnitude), the excitation probabilities ($v' = 1$) display a higher magnitude since the 925 K phonons and surface temperature are more effective for the excitation process compared to the phonons/normal modes obtained from the other approaches investigated to describe the surface.

I. INTRODUCTION

With the advancement of industrial chemical processes employing heterogeneous catalysis, dissociative chemisorption phenomena have been extensively explored through both experimental[1–11] and theoretical[12–40] approaches. At the microscopic level, the dissociation of H_2 and D_2 on Cu surfaces has been specifically investigated as prototypes for understanding chemisorption dynamics. While comprehending complex chemisorption and molecule–surface scattering processes, molecular beam[5–8] and associative desorption[2,3,6,8,10,11] experiments have progressed extensively, which has driven developments in chemically accurate potential energy surface (PES) construction[17,32,35,38,40–44] and exact dynamical methodologies.[13–15,18,22,24–28,30,32–38,40,45,46] State-of-the-art theoretical investigations, namely, quantum dynamics (QD),[29,33,40,46–50] quasi-classical trajectory (QCT),[17,32,34,38,40,44,51,52] and non-equilibrium ring polymer molecular dynamics (NE-RPMD),[53–55] have been carried out on accurate PESs[17,33,34,40,41,44,52,56] to understand the experimental outcomes of molecule–surface scattering phenomena. Moreover, "on-the-fly" force calculation approaches in direct dynamics such as *ab initio* molecular dynamics (AIMD) or density functional theory molecular dynamics (DFMD)[28,33,40,57–59] have also been adopted to bypass PES computation and fitting.

The construction of accurate PESs is crucially important to perform theoretical simulations of dissociative chemisorption and scattering of molecules on and from metal surfaces. Density functionals (DFs) based on the generalized gradient approximation (GGA),[31,40,60,61] combinations of GGA-exchange DFs with correlation DFs,[40,62,63] and *meta*-GGA (mGGA)[40,64] have all been

involved in developing chemically accurate PESs. While constructing such surfaces, major progress has been made through the application of the specific reaction parameter (SRP) approach to density functional theory (DFT) (SRP-DFT),[65,66] leading to SRP-DFT-derived DFs.[17,18,28,35,39,40,51,59,67,68] Moreover, approaches such as embedded correlation wavefunction (ECW)[69] and diffusion Monte Carlo (DMC)[70,71] are also being implemented.[40] For dynamical calculations, the interpolation of *ab initio* electronic structure data is important for constructing continuous functional forms of PESs. The Corrugation Reducing Procedure (CRP) interpolation scheme[41] provides chemically accurate PESs of H_2/D_2 on Cu(111)[18,32,35,38,39,45,60] and H_2/D_2 on Cu(211)[33,40,72,73] facets for calculating dissociative chemisorption and collision processes. On the other hand, neural network (NN) fitted PESs (NNPs)[44,52,56] and high-dimensional NNPs (HD-NNPs) have demonstrated reliability in describing molecule–surface interactions for various prototypes [e.g., CO_2 + Ni(100)/Pt(111)[74,75] and HCl + Au(111)[76]] and highly activated chemisorption reactions [N_2 + Ru(0001)[77] and CHD_3 + Cu(111)[78]]. Zhu and co-workers developed highly transferable PESs using an embedded atom neural network (EANN) approach for H_2/D_2 dissociation on Cu(111)/Cu(100)/Cu(110).[34] The applicability of such HD-NNPs is further explored through 6D quantum dynamics (QD) calculations employing the reactive flux method.[34,61,79]

At non-zero surface temperatures (T_s), dissociation and state-to-state transition probabilities of colliding molecules are (in general) influenced by surface mode vibrations and electron–hole pair (elhp) excitations, which act as energy dissipation channels.[2–11,40,80,81] Electron–hole pair (elhp) excitations influence dissociative chemisorption, inelastic scattering, and phenomena induced by external fields such as vibrational excitation, relaxation, dissipation, and non-adiabatic electron transfer.[40,82–89] Theoretical approaches on electronic friction (EF), independent electron surface hopping (IESH), reduced density matrix, effective Hamiltonian (phonon + elhp), and stochastic wave packet techniques have been utilized to reveal the contributions of elhp excitations to state-to-state vibrational transition probabilities, particularly at higher surface temperatures. AIMDEF-(GLO + LDFA),[59] MDEF-LDFA/ODF,[51] and QD (TDDVR)-EH (phonon + elhp)[90] simulations for H_2/D_2–Cu(111) have, however, shown that elhp excitations contribute negligibly less to the broadening of reaction probabilities compared to surface mode vibrations.

While accurately describing the recoil effect of surface atoms at finite surface temperatures, various theoretical approaches were attempted within the Born–Oppenheimer moving surface (BOMS) model.[81] Among such methods: (a) The *ab initio* molecular dynamics with quantum–classical (AIMD-QC) methods[28,33,40,57] and the quantum mechanics (QM)/metal (Me) embedding approach[91,92] have shown its performance to account for surface temperature effects. (b) To avoid the computational challenges associated with AIMD, quantum–classical trajectory with high-dimensional neural network potential (QCT-HDNNP) calculations[34,44,52,56,74–78] have depicted their effectiveness on computing reaction probabilities. (c) Somers and co-workers have developed the static corrugation model (SCM)[32,35,38] to incorporate the surface temperature effect originating from surface atom displacements and thermal lattice expansion, and simulated the chemisorption dynamics of $H_2(v,j)/D_2(v,j)$ on the Cu(111) surface with both classical and quantum dynamical levels [also computing rovibrational (in-)elastic scattering probabilities].[93,94]

At non-zero surface temperatures (T_s), there are effective Hamiltonian based time-dependent dynamical calculations that attempt to explicitly include the effects of surface mode vibrations or phonon modes: (a) The single oscillator (SO) model,[12,19] through an (single) Einstein oscillator with the Debye vibrational frequency, tries to incorporate the effects of surface temperature, whereas the modified surface oscillator (MSO) model[21,95] introduces local effects of surface atom motion. The theoretical description of surface temperature effects by generalized Langevin oscillator (GLO)[96–98] and modified GLO (MGLO)[99] models has improved to account for the energy dissipation and thermal fluctuations arising from the coupling between the molecule and thermal bath due to surface. These studies were often performed with reduced dimensionality, and comparisons between computed and measured reaction probabilities were made through detailed balance as well as fitting functions. Moreover, there are a limited number of investigations for comparison with state-of-the-art experimental data (and also going beyond comparing reaction probabilities). (b) Jackson and co-workers developed a lattice reconstruction sudden (LRS) model[14,15] to explore the effects of instantaneous responses (e.g., puckering) of lattice atoms [Ni(111)/Ni(211)/Pt(111)] on the dissociation of CH_4 molecules.[49,50,58,100–102] Furthermore, Jackson investigated trapping-mediated dissociation probability for CH_4 chemisorption on Ni(111)/Ir(111)/Pt(111).[103,104] (c) Adhikari and co-workers[23–27,36,90,105,106] formulated a time- and temperature-dependent effective Hartree potential (EHP) within mean-field approximation from linear vibration–translation (VT) molecular DOFs–surface modes couplings incorporating solutions of a linearly forced harmonic oscillator (LFHO)[107] and introducing vibrational density of states (and their population) at a specific surface temperature through Maxwell–Boltzmann (MB) or Bose–Einstein (BE) statistics. This specific effective Hamiltonian approach was used to investigate the effect of surface temperature on $H_2(v,j)/D_2(v,j)$ dissociation due to scattering from Cu(1nn)/Ni(100) surfaces using six-dimensional (6D) and 4D ⊗ 2D quantum dynamics (QD) [time-dependent discrete variable representation (TDDVR)[16,24–27,46]] calculations. This many-oscillator model was also extended[37] beyond the linear coupling by including both linear (VT) and quadratic (anharmonic) vibration–vibration (VV) couplings among molecular DOFs and surface mode vibrations. It showed significant effects of BE vibrational state distribution and anharmonic (quadratic-VV) molecular DOFs–surface modes couplings on the reaction/transition probabilities of $D_2(v=0, j=0,2)$ dissociating on/scattering from the Cu(111) surface at high surface temperatures (T_s = 925 K).

In a recent investigation, Adhikari and co-workers[36,106] utilized the first-principles-based many oscillator linear VT coupling model within the mean-field approach[24–27] using a chemically accurate static corrugation model (SCM)[32] to depict the effect of surface temperature on the dissociation and scattering dynamics of H_2/D_2 ($v=0, j=0$) on Cu(111). When such an effective Hamiltonian is modeled using the SRP48 functional[17] within a cluster approximation, the 6D quantum dynamics (QD) using a split operator (SPO)-DVR method[29,108] displays significant contributions from surface mode degrees of freedom (DOFs) with the inclusion of the quantum state (BE) distribution of surface vibrational modes.[24–27] It

appears that at a high surface temperature, over the range of collision energies, the use of a chemically accurate SCM potential and quantum statistics for the surface modes (BE) were identified as crucial factors leading to broadening of reaction probabilities.

In this present work, the effect of the quantization of the dynamics of the surface is investigated on the reaction probability of the $H_2(v = 0, j = 0)$–Cu(111) system at a surface temperature of 925 K using SRP48 functional based frequencies and displacement vectors for (a) normal modes obtained from cluster approximation and (b) phonons of slabs calculated at 0 and 925 K. In the construction of CRP fitted BOSS PES, we have used two versions, namely, one for a 0 K perfect lattice, which does not account for the thermal expansion effects, and another for a 925 K thermally expanded lattice.[109] The former is employed for the cluster and the 0 K phonon based Hamiltonians, whereas the latter is utilized for the 925 K phonons case. For all these situations, the corresponding effective Hamiltonians formulated by using the first principles-based many oscillator models[16,23–27] relying on a mean-field approximation with a chemically accurate SCM[32] potential are employed to perform scattering calculations using the split operator (SPO)-DVR QD code.[29] It may be noted that (a) molecular (H_2) degrees of freedom (DOFs) and surface [Cu(111)] modes interaction potential, and its first derivatives are obtained from the SCM potential and (b) surface temperature is incorporated by considering BE probability factors for the initial state distribution of modes. All these calculated results will be compared to the calculations performed on the 0 K perfect crystal (RS) and the experimentally measured reaction probability profiles obtained by Kaufmann and co-workers.[11]

II. THEORETICAL BACKGROUND

The time- and temperature-dependent effective Hamiltonian includes the effects of quantization on the surface dynamics of a diatomic molecule scattering from a metal surface under non-zero surface temperature conditions, where the quantized states of normal modes or phonons representing the surface are distributed by BE statistics and the interactions between molecular DOFs and surface modes are included by considering chemically accurate SCM potential. Such a formulation has a limited correlation between the molecular degrees of freedom ($\{\chi_m\}$) and surface vibrational modes ($\{Q_k\}$), supported by the substantial mass disparity between the diatomic molecule (H_2/D_2) and surface atoms (Cu), which is known as mean-field approximation. In other words, the total system is defined by a wavefunction of the Hartree product type,[24–27,36,37,106]

$$\Psi_{\text{diatom}}(x, y, z, X, Y, Z, t) \cdot \Phi_{\text{vib}}(\{Q_k\}, t), \tag{1}$$

where the six degrees of freedom for the diatomic molecule ($\{\chi_m\} \equiv \{x, y, z, X, Y, Z\}$) are denoted into two sets of Cartesian coordinates: (x, y, z) representing the molecular vector [$\mathbf{r} = (x, y, z)$] and (X, Y, Z) representing the center of mass (COM) [$\mathbf{R} = (X, Y, Z)$]

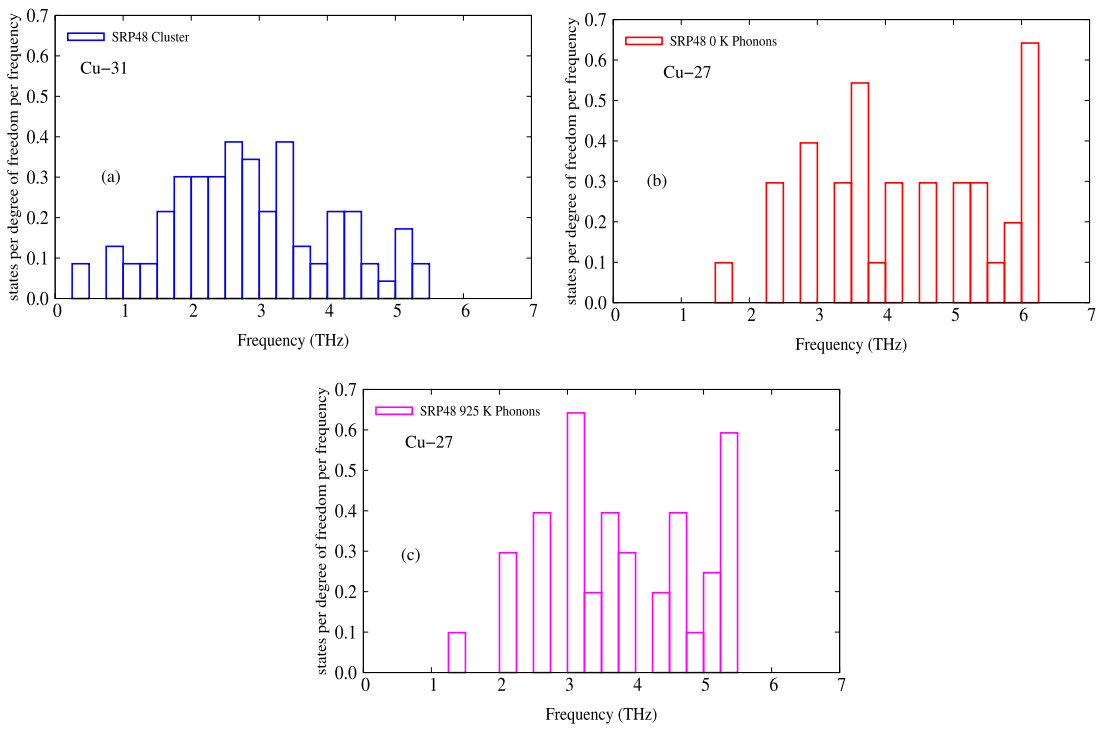

FIG. 1. SRP48 functional based frequency distribution spectrum of (a) cluster model computed with a cluster approximation using 31 atoms and (b) and (c) phonons of the slab calculated at 0 and 925 K, respectively, both using 27 Cu atoms.

positions of the molecule with respect to the top layer of the metal (Cu) surface (located at $Z = 0$). We investigate different models to describe the surface vibrational modes $\{Q_k\}$: (i) a cluster consisting of 31 atoms and (ii) slabs consisting of 3×3 multiples of the unit cell of the Cu(111) surface, one based on the lattice constant at 0 K and one accounting for the experimentally determined lattice expansion at 925 K.[42] The cluster model has already been used in our previous work and yields harmonic normal modes as described therein.[36,106] Phonons are calculated for the slab models according to the harmonic approximation at 0 K and the quasi-harmonic approximation at 925 K as implemented in the phonopy package.[110,111] For both the normal mode and the phonon calculations, the SRP48 DFT functional available in an in-house version of the VASP code[17] is employed. The associated frequency spectra ($\{\omega_k\}$) resulting from these calculations are shown in Fig. 1. More details on the phonon calculations are going to be the subject of a forthcoming publication.[112] The surface vibrational mode coordinates ($\{Q_k\}$) are provided in Sec. S1 of the supplementary material.

When the product type wavefunction [Eq. (1)] is substituted in TDSE and surface modes are integrated out over the configuration space, the time- and temperature-dependent six-dimensional effective Hamiltonian (EH) for the incoming molecule arrives[24–27,36,37,106] in the following form:

$$\begin{aligned}\widehat{H}(\{\chi_m\}, T_s) = &-\frac{\hbar^2}{2\mu}\left(\frac{\partial^2}{\partial x^2} + \frac{\partial^2}{\partial y^2} + \frac{\partial^2}{\partial z^2}\right) \\ &- \frac{\hbar^2}{2M}\left(\frac{\partial^2}{\partial X^2} + \frac{\partial^2}{\partial Y^2} + \frac{\partial^2}{\partial Z^2}\right) \\ &+ V_0(\{\chi_m\}) + V_{eff}^{\text{vib}}(\{\chi_m\}, t, T_s),\end{aligned} \tag{2}$$

where the reduced mass (μ) and total mass (M) of the diatomic molecule are explicitly incorporated in the kinetic energy (KE) terms. The PES, $V_0(\{\chi_m\})$, defines the BOSS interaction for the RS, representing an ideal static lattice with no contribution from surface vibrational degrees of freedom. On the contrary, the time- and temperature-dependent EHP, $V_{eff}^{\text{vib}}(\{\chi_m\}, t, T_s)$, originates due to the interactions between molecular DOFs and surface vibrational modes.

It is expected that this EHP will affect the incoming diatomic molecule throughout the scattering process, particularly under finite surface temperature conditions ($T_s \neq 0$ K). The time evolution of molecular DOFs is carried out through 6D QD calculations employing single wavepacket propagation, which represents a pure state description for the molecule. On the other hand, at a finite surface temperature, the collective effects of molecular DOFs–surface modes couplings on the projectile motion are incorporated by constructing a time- and temperature-dependent EHP, where the BE or MB probability distributions facilitate an ensemble average over vibrational state configurations of surface modes leading to a mixed state. In other words, the scattering matrix (S), which is being computed with the initial and final states of the H_2 molecule, remains the same (independent of pure state or density matrix based propagation), since the time- and temperature-dependent effect of surface vibrational modes on molecular DOFs–surface interaction is incorporated into the effective Hamiltonian by integrating out the density of states involved with each surface vibrational mode by employing a mean field approach. If the recoil energy of surface becomes significant, the higher order correlation between molecular- and surface-DOFs wavefunctions could be important and the mean field approach will collapse, but at present, the recoil effect is expected to be minimal due to the large mass difference between the incoming gas molecule (H_2) and the surface atom (Cu). Such an approach allows for an "accurate" representation of the initial conditions in molecular beam experiments.

A. Formulated EHP (V_{eff}^{vib})

While averaging over the initial vibrational state configuration ($\{n_0\}$) of a set of surface modes or phonons ($\{k\}$), the time- and temperature-dependent EHP can be expressed as[36,37]

$$V_{eff}^{\text{vib}}(\{\chi_m\}, t, T_s) = \langle V\rangle^{\text{vib}}(t, T_s) = \sum_{\{n_0\}} p_{\{n_0\}} \langle V\rangle_{\{n_0\}}^{\text{vib}}, \tag{3}$$

where $p_{\{n_0\}}$ represents either the quantum (BE) or the classical (MB) probability distribution of a particular vibrational state population ($\{n_0\}$) for the set of normal or phonon modes ($\{k\}$),

$$p_{\{n_0\}} = \prod_{k=1}^{M} p_{n_k^0}^k, \tag{4}$$

where $p_{n_k^0}^k$ is the normalized probability distribution corresponding to the specific normal mode (k) with a particular occupation number (n_k^0).

For a particular state (vibrational) configuration ($\{n_0\}$), the Hartree potential originates from the interaction potential (V_I^{vib}) between molecular DOFs and surface mode vibrations as[36,37]

$$\langle V\rangle_{\{n_0\}} = \langle \Phi_{\text{vib}} | V_I^{\text{vib}} | \Phi_{\text{vib}} \rangle. \tag{5}$$

When the linear molecular DOFs–surface modes coupling is only considered, the state dependent Hartree potential can be defined as[36] (see Sec. S2 of the supplementary material for details)

$$\begin{aligned}\langle V\rangle_{\{n_0\}}^{VT} &= \langle \Phi_{\text{vib}}(t) | V_I^{VT} | \Phi_{\text{vib}}(t) \rangle \\ &= \sum_{\{n'\}} \sum_{\{n\}} \alpha^*_{\{n'\}\leftarrow\{n_0\}}(t) \alpha_{\{n\}\leftarrow\{n_0\}}(t) \langle \{n'\} | V_I^{VT} | \{n\} \rangle,\end{aligned} \tag{6}$$

where $\alpha_{\{n\}\leftarrow\{n_0\}}(t)$ defines the amplitude of a transition evolving from an initial state configuration $\{n_0\}$ to a particular one $\{n\}$ under the VT evolution operator (U_{VT}),

$$\alpha_{\{n\}\leftarrow\{n_0\}}(t) = \langle \{n\} | U_{VT} | \{n_0\} \rangle. \tag{7}$$

While evaluating the integral $\langle \{n'\} | V_I^{VT} | \{n\} \rangle$, the linear VT interaction potential (V_I^{VT}) is expressed in terms of normal or phonon modes (Q_ks) by introducing bosonic operators (b_k, $b_k^\dagger$) as $Q_k = A_k(b_k^\dagger + b_k)$; $A_k = \sqrt{\hbar/2\omega_k}$, which leads to the following form of interaction potential:[36]

$$V_I^{VT} = \sum_k \lambda_k A_k (b_k F_k^- + b_k^\dagger F_k^+) V_{k,1}, \tag{8}$$

where $F_k^+ = \exp(i\omega_k t)$, $F_k^- = \left(F_k^+\right)^*$, and $V_{k,1} = \frac{\partial V_I^{VT}}{\partial Q_k}|_{eq}$.

In Eq. (8), the first derivative of the interaction potential ($V_{k,1}$) with respect to normal/phonon mode (Q_k) is evaluated by using the chemically accurate SCM potential[32] [$V_{a\alpha}^{\mathrm{Cu-H}}$, function of gas (a)–metal (α) atom distance ($r_{a\alpha}$)] with the aid of the chain rule of differentiation with respect to the metal atom position ($X_{\alpha i}$; $\alpha = 1, 2, \ldots, N$; $i \equiv$ specific direction) as follows:[36]

$$V_{k,1} = \left(\frac{\partial V_I^{VT}}{\partial Q_k}\right) = \sum_{a\alpha} \frac{\partial (V_{a\alpha}^{\mathrm{Cu-H}}(r_{a\alpha}) - V_{a\alpha}^{\mathrm{Cu-H}}(r_{a\alpha}^{\mathrm{id}}))}{\partial Q_k} = \sum_{a\alpha i} \left[\frac{\partial V_{a\alpha}^{\mathrm{Cu-H}}(r_{a\alpha})}{\partial X_{\alpha i}} - \frac{\partial V_{a\alpha}^{\mathrm{Cu-H}}(r_{a\alpha}^{\mathrm{id}})}{\partial X_{\alpha i}}\right] \cdot \frac{\partial X_{\alpha i}}{\partial Q_k} = \sum_{a\alpha i} m_\alpha^{-1/2} \left[\frac{\partial V_{a\alpha}^{\mathrm{Cu-H}}(r_{a\alpha})}{\partial X_{\alpha i}} - \frac{\partial V_{a\alpha}^{\mathrm{Cu-H}}(r_{a\alpha}^{\mathrm{id}})}{\partial X_{\alpha i}}\right] T_{\alpha i;k}, \tag{9}$$

where $r_{a\alpha}^{\mathrm{id}}$ represents the gas–metal atom distance for an undisplaced (ideal) metal atom. $\{T_{\alpha i;k}\}$ defines the transformation matrix elements between the local ($\{X_{\alpha i}\}$) and normal/phonon modes ($\{Q_k\}$; $k = 7, 8, \ldots, 3N$) as $X_{\alpha i} - X_{\alpha i}^{\mathrm{id}} = m_\alpha^{-1/2} \sum_k T_{\alpha i;k} Q_k$ and m_α = mass of a metal atom. In Sec. S3 of the supplementary material, the details of the derivative of SCM potential with respect to metal atom position ($\frac{\partial V_{a\alpha}^{\mathrm{Cu-H}}(r_{a\alpha})}{\partial X_{\alpha i}}$) are shown.[36]

While inserting Eqs. (8) and (6) in Eq. (3) along with the quantum (BE) or the classical (MB) vibrational state distribution, the time and temperature 6D ($\{\chi_m\} \equiv \{x, y, z, X, Y, Z\}$) EHP takes the following form within the linear VT molecular DOFs–surface modes coupling model[36] (see Sec. S2 of the supplementary material for details):

$$V_{\mathrm{eff,BE}}^{VT}(\{\chi_m\}, t, T_s) = \frac{1}{N_{\mathrm{BE}}} \left[\sum_{k=7}^{3N} \lambda_k \frac{1}{\omega_k^2} V_{k,1}^2(\{\chi_m\}) [\cos \omega_k (t - t_0) - 1] \sum_{q=1}^{\infty} \frac{z_k^{q/2}}{(1 - z_k^q)}\right], \quad \text{BE case,} \tag{10a}$$

or

$$V_{\mathrm{eff,MB}}^{VT}(\{\chi_m\}, t, T_s) = \frac{1}{N_{\mathrm{MB}}} \left[\sum_{k=7}^{3N} \lambda_k \frac{1}{\omega_k^2} V_{k,1}^2(\{\chi_m\}) [\cos \omega_k (t - t_0) - 1] \frac{z_k^{1/2}}{(1 - z_k)}\right], \quad \text{MB case,} \tag{10b}$$

where $N_{\mathrm{BE}} \left(= \sum_k \sum_{q=1}^{\infty} \frac{(z_k)^{\frac{q}{2}}}{(1-z_k^q)}\right)$ and $N_{\mathrm{MB}} \left(= \sum_k \frac{z_k^{\frac{1}{2}}}{(1-z_k)}\right)$ denotes the normalization factors of the BE and MB probability distributions, respectively. Both for the BE and MB cases, the form of EHPs is explicitly dependent on the surface mode frequencies ($\{\omega_k\}$) as well as on time appearing due to the $\cos \omega_k (t - t_0)$ term, where the factors $\sum_{q=1}^{\infty} \frac{z_k^{q/2}}{(1-z_k^q)}$ for the BE distribution and $\frac{z_k^{1/2}}{(1-z_k)}$ for the MB distribution, show the temperature as a parameter: $[z_k = \exp(-\frac{\hbar \omega_k}{k_B T})]$.

Recently, the applicability of such a many oscillator-SCM model combined with the BE or MB probability distribution of vibrational states for describing the surface temperature effect for the $H_2(v = 0, j = 0)$-Cu(111),[36] as well as the $D_2(v = 0, j = 0)$-Cu(111)[106] dissociative scattering system, has been explored by carrying out 6D QD calculations with the SPO-DVR code.[29,108] The EHP (VT; SCM) has enabled a considerable broadening of reaction probabilities at moderate as well as higher surface temperatures with respect to the RS (BOSS) ($T_s = 0$ K) situation.[36,106]

B. Mean-field approach and sudden approximation

The couplings among molecular DOFs and surface mode vibrations are assumed to be responsible for the effect of surface temperature on dissociative scattering processes, where theoretical schemes such as sudden approximation and mean-field approach are employed to describe such processes quantitatively as sudden approximation[14,15,49,50,100–103] based approaches take into account the effect of surface atom vibrations through the MB (or even BE) distribution of the lattice vibrational DOF (Q). While performing dynamics within sudden approximation, it employs a unique surface for the entire scattering process, but this procedure is repeated for surfaces generated by the other configuration spaces obtained through the BE or MB distribution functions. On the other hand, the mean-field approximation based Hartree product-type wavefunction has been used to construct the EHP,[24–27,36,37,90,105] which includes the coupling between molecular DOFs and surface modes. In the case of scattering dynamics with EHP, it considers time averaged PESs since the space dependent Hartree potential is modified by the product of a time dependent expression in terms of the frequencies of surface vibrations. As a result, both mean-field and sudden approximations can encapsulate the correlations among molecular DOFs and surface mode vibrations arising at a particular surface temperature at different levels of theory. The applicability of both methods to calculate the chemisorption as well as scattering dynamics of the specific system(s) could be verified only by constructing models based on those approaches and carrying out dynamics.

C. Computational details: QD-EH methodology

The EHP is defined by expressions involving derivatives of the interaction potential with respect to normal/phonon modes ($\{V_{k,1}\}$; $V_{k,1} = \frac{\partial V_I^{VT}}{\partial Q_k}$), surface mode frequencies ($\{\omega_k\}$), a time-dependent term ($[\cos \omega_k (t - t_0) - 1]$), and the temperature-dependent terms related to the BE and MB probability factors ($\sum_{q=1}^{\infty} \frac{z_k^{q/2}}{(1-z_k^q)}$ for BE, $\frac{z_k^{1/2}}{(1-z_k)}$ for MB), which are presented in details by Eqs. (10a) and (10b). The computation of derivatives of the interaction potential ($\{V_{k,1}\}$) relies on the chemically accurate SCM potential, using a transformation matrix ($\{T_{\alpha i;k}\}$) connecting local ($X_{\alpha i}$) and normal modes ($\{Q_k\}$). In the EH framework, a 6D QD simulation for H_2 on Cu(111) is conducted, initializing the hydrogen molecule in its rovibrational ground state ($v = 0, j = 0$). At low collision energies, both for RS (0 K perfect lattice) and non-zero surface temperatures, unphysical oscillations in the reaction probability profiles[36,106] are possibly attributed to larger time steps, shorter total propagation times, or the reflection of wavepackets due to optimal positions of analysis points and optical potentials in the SPO-DVR[29,108] dynamics, which are required to obtain computational efficiency. The associated dynamical parameters are optimized and presented in Sec. S4 of the supplementary material.

III. RESULTS AND DISCUSSION

The dynamics and analysis focus on computing the reaction and scattering probabilities of $H_2(v = 0, j = 0)$ on the Cu(111) system at a specific surface temperature (T_s = 925 K) using various kinds of Hartree potentials [based on the different approaches to model the solid] as described below. In this calculation, we intend to carry out scattering dynamics employing Hartree potential constructed at 925 K surface temperature with the frequency spectrum ($\{\omega_k\}$) and displacement vector ($\{T_{\alpha i;k}\}$) of surface atoms calculated by various levels of approximation, namely, SRP48 functional based normal modes within cluster approximation and phonons obtained by slab calculation at 0 and 925 K. While constructing such Hamiltonians, we employ (a) the gas–surface interaction potential (CRP fitted BOSS PES)[41] for 0 K perfect and 925 K thermally expanded lattice metal atom coordinates and (b) the interaction potential (SCM)[32] between the gas and the metal atoms due to the surface atom vibrations. In our present calculations, both of these interaction potentials are brought into the same coordinate framework to include the effect of cluster/phonon modes in the Hamiltonian at a non-zero surface temperature. This was not done previously.[36,106]

A. Reaction probability

The BE or MB probability factors are employed for the initial state distribution of surface vibrational DOFs to construct the Hartree potentials at a non-zero surface temperature. The vibrational DOFs are obtained by various approaches, namely, (i) a cluster approximation and (ii) two slab calculations, one based on phonons from a 0 K perfect crystal lattice and another based on phonons from a 925 K (thermally expanded) lattice (where also a corresponding 925 K BOSS PES was constructed for the H_2 on Cu interaction).[109] In Fig. 2, we present the reaction probabilities at a 925 K surface temperature for the dissociation of $H_2(v = 0, j = 0)$ on the Cu(111) surface in comparison with the RS (0 K ideal lattice) profile. In the case of the cluster approximation, the reaction probability profile calculated at a surface temperature of 925 K shows negligible effects for the MB case compared to the RS calculated probabilities. However, for the BE case, the profile shows significant broadening [see Fig. 2(a)]. At a 925 K surface temperature, similar results can be seen for the Hartree potential constructed with 0 K phonons, where no broadening is observed for the MB case, but the BE reaction probability profile depicts considerable broadening [see Fig. 2(b)]. Moreover, when scattering calculations are performed at 120 and 925 K surface temperatures on the Hartree potential constructed with the 0 K phonons and compared with each other, it appears in Fig. S1 of the supplementary material that the BE reaction probabilities at 925 K are much higher than the corresponding 120 K case over the entire collisional energy domain. On the other hand, when the reaction probabilities are computed with the 925 K phonons for a surface temperature of 925 K, both the BE and MB profiles show significant broadening compared to the RS case [see Fig. 2(c)], and broadening

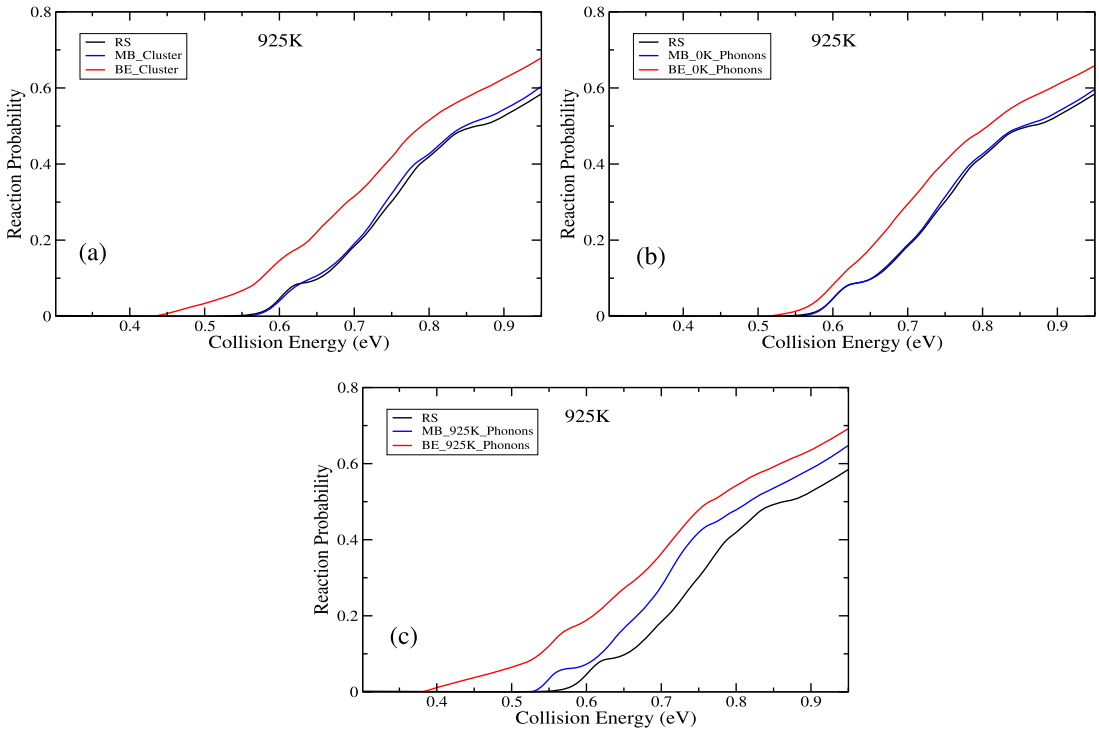

FIG. 2. Comparison of reaction probabilities for the H_2 on Cu(111) with the MB and the BE probability factors at a 925 K surface temperature calculated using the Hartree potential constructed with (a) cluster based normal modes, (b) and (c) phonons of slab at 0 and 925 K frequencies and compared with the RS case (0 K ideal lattice).

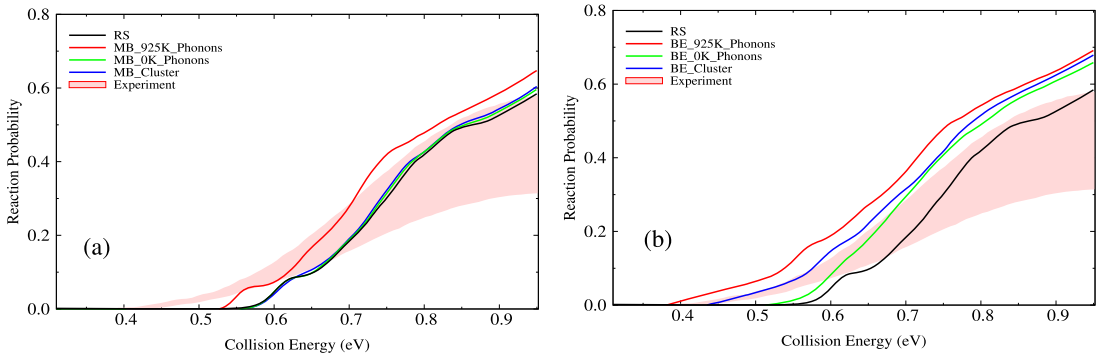

FIG. 3. Reaction probabilities for the H_2 on Cu(111) based on the RS and EHP constructed with the VASP-SRP48 calculated normal mode frequencies for a 925 K surface temperature, where plots (a) and (b) depict the MB and BE probability factors, respectively, with $(\{V_{k,1}\})$ set to zero if magnitude is $\leq 1.0 \times 10^{-10}$.

for the BE is more compared to the MB case again. As a matter of fact, the reaction probabilities calculated by employing various kinds of Hartree potentials constructed with different levels of calculated surface vibrational DOFs depict substantial differences depending on the use of statistics (BE or MB) for the initial state distribution of normal modes/phonons at a specific surface temperature. Such a difference is clearly predictable from the MB or BE probability factors as a function of surface vibrational frequencies, as shown in Fig. S2 of the supplementary material.

While summarizing the above results, in Figs. 3(a) and 3(b), reaction probability profiles are presented for the above mentioned three approaches that are formulated with differently calculated surface vibrational DOFs and derived with MB or BE probability factors, respectively, in comparison with RS (0 K perfect crystal) and experimental data,[11] whereas the thresholds of reaction probability for those profiles are depicted in Table I. The reaction probability profiles calculated at non-zero surface temperature depict lower and higher collisional energy shifts of the threshold for the BE and MB cases, respectively, compared to the RS case. Indeed, among the reaction probability profiles obtained from the Hartree potential constructed with the MB probability factor, only the profile computed with 925 K phonons and surface temperature depicts reasonable broadening compared to the RS case, while such an effect is negligibly small for other MB cases. On the contrary, as discussed earlier, all the reaction probability profiles evaluated using the BE probability factor show broadening across the entire energy domain, where in the case of 925 K phonons and surface temperature calculation, the effect is most prominent. It is interesting to note that at the lower collisional energy regime, the BE profiles show closer agreement, particularly near the threshold with the experimental[11] data compared to the MB situations, and that is thus because of the thermal expansion being included now correctly into the model by using also the 925 K BOSS PES together with the 925 K phonons (see Table I).

B. State-to-state scattering probability

At a 925 K surface temperature, Fig. 4 depicts the profiles of vibrational state-to-state scattering probabilities of the scattered $H_2(v' = 0, 1)$ molecule. The chemisorption probability for the RS (0 K BOSS) is consistently lower than in all other approaches at non-zero surface temperatures, resulting in the highest survival $(v' = 0)$ and excitation $(v' = 1)$ probabilities at any given collisional energy. On the other hand, for the 925 K phonon and surface temperature calculation, the magnitude of survival transition probability $[H_2(v' = 0)]$ is the lowest compared to other approaches for the entire collisional energy domain. This is expected as the chemisorption reaction probabilities depict the largest magnitude for the 925 K phonon and surface temperature calculation compared to the other approaches [see Fig. 3(b)]. On the contrary, even though the excitation probabilities $(v' = 1)$ for all the calculations of different cases

TABLE I. Comparative threshold energy values are obtained for the BE and MB cases, for the different approaches used for the H_2 on Cu(111) systems in this work.

Method	Surface temperature (K)	CRP potential	Threshold energy (eV) BE	Threshold energy (eV) MB
SRP48 925 K phonons	925	925 K BOSS PES[109]	0.384	0.527
SRP48 cluster	925	0 K BOSS PES	0.436	0.557
SRP48 0 K phonons	925	0 K BOSS PES	0.514	0.556
QD-BOSS	⋯	0 K BOSS PES	0.496	
Experiment[11]	925		0.392	

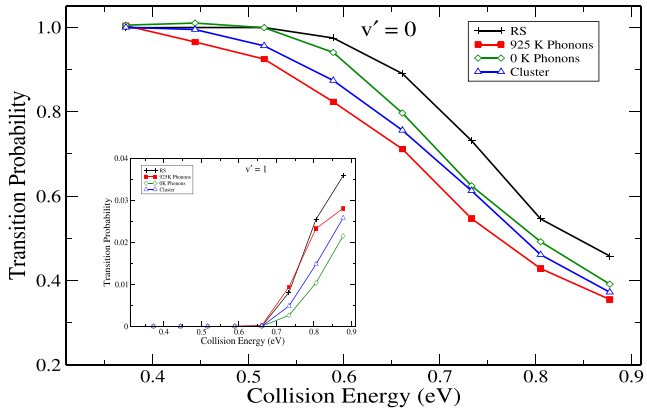

FIG. 4. Energy-resolved state-to-state vibrationally elastic and inelastic transition probabilities are depicted.

are very low, those for the 925 K phonons and surface temperature are generally higher than other non-zero surface temperature calculations, and again, this is because for this case the thermal lattice expansion is now included in both the phonons and in the used 925 K BOSS PES. The thermally expanded lattice lowers the barrier to reaction.[32] On the other hand, at a particular collisional energy of 0.877 eV (with the highest collisional energy, the transfer of energy from metal to molecular DOFs increases so that a substantial amount of probabilities for higher rotational as well as vibrational states are included), in Fig. 5, transition probabilities for the scattered $H_2(v' = 0/1, j')$ molecule as a function of rotational states j' are presented. In both cases, $H_2(v' = 0, j')$ and $H_2(v' = 1, j')$, the rotational transition probabilities show a maximum around $j' = 2$ for all four approaches. These distributions of roto-vibrational probabilities clearly demonstrate the same features and mechanisms as we have discussed for survival and excitation probabilities.

IV. CONCLUSION

Within the mean field approximation, we derive the EHP by considering the gas–metal atom interaction potential, where the analytic form of the derivative of SCM potential[32] with respect to normal (cluster)/phonon (slab) modes gets into the explicit expression through an ensemble average over the initial states of those modes with BE or MB probability factors. Such an effective Hamiltonian contains the following terms: $\{V_{k,1}\}(V_{k,1} = \frac{\partial V_I^{VT}}{\partial Q_k})$, surface mode frequencies $(\{\omega_k\})$, a time-dependent term $([\cos\omega_k(t - t_0) - 1])$, and the temperature-dependent terms related to BE and MB probability factors $(\sum_{q=1}^{\infty} \frac{z_k^{q/2}}{(1-z_k^q)}$ for BE, $\frac{z_k^{1/2}}{(1-z_k)}$ for MB). Even though the general expression of EHPs are the same, it differs depending on the choice of the normal/phonon modes (and which BOSS PES is used), and thereby, there are three different approaches to construct the effective potential, differing in how the phonons are computed and the thermal lattice expansion is included in the calculations. With these EHPs, we perform 6D QD with SPO-DVR[29,108] dynamics for H_2 on Cu(111) initializing the hydrogen molecule in its rovibrational ground state $(v = 0, j = 0)$.

These dynamical calculations are carried out to compute the reaction and scattering probabilities of $H_2(v = 0, j = 0)$ on the Cu(111) system at a specific surface temperature (T_s = 925 K) using various kinds of Hartree potentials constructed with SRP48 functional based normal modes within cluster approximation and phonons obtained by slab calculation at 0 and 925 K. It needs to be mentioned that in constructing the EHP, the origins of the coordinate systems for gas–metal distance to define the RS interaction potential (CRP)[41] as well as the interaction potential (SCM)[32] to include the vibration of the metal atoms at a finite temperature are taken to be the same, contrary to our earlier construction of the EHP.[36,106]

The present calculations depict that for 925 K phonons and surface temperature, chemisorption probabilities are higher over the entire energy domain compared to other EHP based calculations, whereas it has the threshold reaction probabilities at the lowest collisional energy with respect to other calculations as well as the RS (0 K perfect lattice) calculation, but it agrees quite well with experimental[11] threshold energy. This could be due to the inclusion of four physical phenomena: (i) the use of 925 K phonons calculated from a slab, (ii) the incorporation of lattice expansion through 925 K CRP potential, (iii) engaging BE statistics over MB, and (iv) overall, the

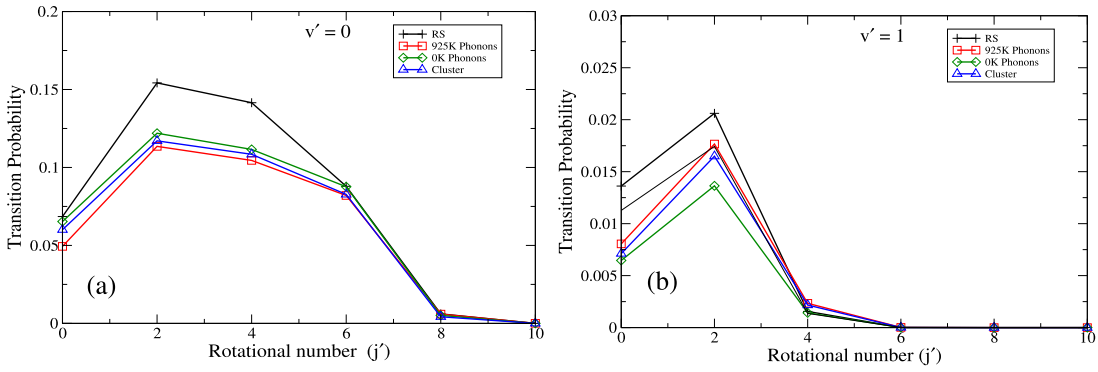

FIG. 5. At a collisional energy of 0.877 eV, the rotational transition probabilities of the scattered (a) $H_2(v' = 0, j')$ and (b) $H_2(v' = 1, j')$ molecules from the Cu(111) surface for the RS case and a 925 K surface temperature are computed as a function of the rotational state (j').

H_2 dissociation barrier for an expanded 925 K PES might be lower than for a 0 K BOSS PES.[32,45,94,109] At the same time, for such Hartree potential constructed with 925 K phonons as well as 925 K surface temperature, the corresponding survival probability ($v' = 0$) is the lowest over the energy domain compared to the other approaches employed to formulate Hartree potential. On the contrary, the excitation probabilities ($v' = 1$) depict the opposite trend compared to the other approaches, presumably due to such phonons calculated at 925 K with a surface temperature of 925 K, which are more active in the excitation process. In summary, the present approach with "correctly" calculated phonons, including thermal lattice expansion, and using the proper BE statistics can mimic the experimental situation much better, depicting appropriate mechanistic insight.

SUPPLEMENTARY MATERIAL

See the supplementary material for details regarding (a) the SRP48 functional based cluster and phonons of slab at 0 and 925 K calculations of vibrational frequencies and displacement vectors [optimized structure, normal mode frequencies, and displacement vectors are presented in a `.xyz` file (displayed in a `.pdf` file)], (b) the formulation of time and temperature dependent EHP for linear molecular DOFs–surface modes couplings, (c) the derivative of SCM interaction potential with respect to metal atom position, and (d) the SPO-DVR dynamical parameters for 6D QD-RS(BOSS) ($T_s = 0$ K) and 925 K reaction probability profiles of $H_2(v = 0, j = 0)$ scattering/dissociating on the Cu(111) surface.

ACKNOWLEDGMENTS

M.K.S. acknowledges the NBCFDC, Govt. of India, Ministry of Social Justice and Empowerment, for the research fellowship. K.N. acknowledges the IACS for the research fellowship. S.A. acknowledges DST-SERB, India, for research funding under Project No. CRG/2023/000611 and thanks the IACS for access to the supercomputing facility. B.S., J.M., and M.F.S. acknowledge the financial support from the Netherlands Organization for Scientific Research (NWO).

AUTHOR DECLARATIONS

Conflict of Interest

The authors have no conflicts to disclose.

Author Contributions

Mantu Kumar Sah: Conceptualization (supporting); Investigation (supporting); Project administration (supporting); Software (equal); Writing – original draft (lead); Writing – review & editing (equal). **Koushik Naskar**: Investigation (supporting); Software (supporting). **Satrajit Adhikari**: Conceptualization (lead); Investigation (lead); Methodology (lead); Project administration (lead); Software (supporting); Writing – original draft (supporting); Writing – review & editing (lead). **Bauke Smits**: Conceptualization (supporting); Methodology (supporting); Project administration (supporting); Writing – review & editing (supporting). **Jörg Meyer**: Conceptualization (supporting); Project administration (supporting); Writing – review & editing (supporting). **Mark F Somers**: Methodology (supporting); Project administration (supporting); Writing – review & editing (supporting).

DATA AVAILABILITY

The data that support the findings of this study are available within the article and its supplementary material.

REFERENCES

[1] E. Watts and G. O. Sitz, J. Chem. Phys. **114**, 4171 (2001).
[2] H. A. Michelsen, C. T. Rettner, D. J. Auerbach, and R. N. Zare, J. Chem. Phys. **98**, 8294 (1993).
[3] H. A. Michelsen and D. J. Auerbach, J. Chem. Phys. **94**, 7502 (1991).
[4] H. A. Michelsen, C. T. Rettner, and D. J. Auerbach, Surf. Sci. **272**, 65 (1992).
[5] C. T. Rettner, H. A. Michelsen, and D. J. Auerbach, Faraday Discuss. **96**, 17 (1993).
[6] C. T. Rettner, H. A. Michelsen, and D. J. Auerbach, J. Chem. Phys. **102**, 4625 (1995).
[7] C. T. Rettner, H. A. Michelsen, and D. J. Auerbach, Chem. Phys. **175**, 157 (1993).
[8] C. T. Rettner, D. J. Auerbach, and H. A. Michelsen, Phys. Rev. Lett. **68**, 1164 (1992).
[9] H. Hou, S. J. Gulding, C. T. Rettner, A. M. Wodtke, and D. J. Auerbach, Science **277**, 80 (1997).
[10] M. J. Murphy and A. Hodgson, J. Chem. Phys. **108**, 4199 (1998).
[11] S. Kaufmann, Q. Shuai, D. J. Auerbach, D. Schwarzer, and A. M. Wodtke, J. Chem. Phys. **148**, 194703 (2018).
[12] Z. S. Wang, G. R. Darling, and S. Holloway, Phys. Rev. Lett. **87**, 226102-1 (2001).
[13] S. Nave and B. Jackson, Phys. Rev. Lett. **98**, 173003-1 (2007).
[14] A. K. Tiwari, S. Nave, and B. Jackson, Phys. Rev. Lett. **103**, 253201-1 (2009).
[15] A. K. Tiwari, S. Nave, and B. Jackson, J. Chem. Phys. **132**, 134702 (2010).
[16] G. D. Billing, Phys. Chem. Chem. Phys. **4**, 2865 (2002).
[17] C. Díaz, E. Pijper, R. A. Olsen, H. F. Busnengo, D. J. Auerbach, and G. J. Kroes, Science **326**, 832 (2009).
[18] C. Díaz, R. A. Olsen, D. J. Auerbach, and G. J. Kroes, Phys. Chem. Chem. Phys. **12**, 6499 (2010).
[19] M. Hand and J. Harris, J. Chem. Phys. **92**, 7610 (1990).
[20] A. C. Luntz and M. Persson, J. Chem. Phys. **123**, 074704-1 (2005).
[21] M. Dohle and P. Saalfrank, Surf. Sci. **373**, 95 (1997).
[22] F. Luder, M. Nest, and P. Saalfrank, Theor. Chem. Acc. **127**, 183 (2010).
[23] S. Adhikari and G. D. Billing, J. Chem. Phys. **112**, 3884 (2000).
[24] T. Sahoo, S. Sardar, and S. Adhikari, Phys. Chem. Chem. Phys. **13**, 10100 (2011).
[25] T. Sahoo, S. Sardar, P. Mondal, B. Sarkar, and S. Adhikari, J. Phys. Chem. A **115**, 5256 (2011).
[26] T. Sahoo, S. Sardar, and S. Adhikari, Phys. Scr. **84**, 028105 (2011).
[27] T. Sahoo, S. Mukherjee, and S. Adhikari, J. Chem. Phys. **136**, 084306-1 (2012).
[28] F. Nattino, A. Genova, M. Guijt, A. S. Muzas, C. Díaz, D. J. Auerbach, and G. J. Kroes, J. Chem. Phys. **141**, 124705 (2014).
[29] M. D. Feit, J. A. Fleck, and A. Steiger, J. Comput. Phys. **47**, 412 (1982).
[30] B. Jackson and S. Nave, J. Chem. Phys. **135**, 114701 (2011).
[31] T. Liu, B. Fu, and D. H. Zhang, J. Chem. Phys. **141**, 194302 (2014).
[32] M. Wijzenbroek and M. F. Somers, J. Chem. Phys. **137**, 054703 (2012).
[33] G.-J. Kroes and C. Díaz, Chem. Soc. Rev. **45**, 3658 (2016).
[34] L. Zhu, Y. Zhang, L. Zhang, X. Zhou, and B. Jiang, Phys. Chem. Chem. Phys. **22**, 13958 (2020).
[35] P. Spiering, M. Wijzenbroek, and M. F. Somers, J. Chem. Phys. **149**, 234702 (2018).
[36] J. Dutta, S. Mandal, S. Adhikari, P. Spiering, J. Meyer, and M. F. Somers, J. Chem. Phys. **154**, 104103 (2021).

[37]J. Dutta, S. Mandal, and S. Adhikari, Chem. Phys. **552**, 111371 (2022).
[38]B. Smits and M. F. Somers, J. Chem. Phys. **154**, 074710 (2021).
[39]E. W. F. Smeets and G.-J. Kroes, Phys. Chem. Chem. Phys. **23**, 7875 (2021).
[40]G.-J. Kroes, Phys. Chem. Chem. Phys. **23**, 8962 (2021).
[41]H. F. Busnengo, A. Salin, and W. Dong, J. Chem. Phys. **112**, 7641 (2000).
[42]F. Nattino, C. Díaz, B. Jackson, and G.-J. Kroes, Phys. Rev. Lett. **108**, 236104 (2012).
[43]G.-J. Kroes, J. Phys. Chem. Lett. **6**, 4106 (2015).
[44]X. Zhou, Y. Zhang, R. Yin, C. Hu, and B. Jiang, Chin. J. Chem. **39**, 2917 (2021).
[45]M. Bonfanti, M. F. Somers, C. Díaz, H. F. Busnengo, and G.-J. Kroes, Z. Phys. Chem. **227**, 1397 (2013).
[46]S. Mandal, S. Ghosh, S. S. Sardar, and S. Adhikari, Int. Rev. Phys. Chem. **37**, 607 (2018).
[47]Y. Huang, W. Zhu, D. J. Kouri, and D. K. Hoffman, Chem. Phys. Lett. **206**, 96 (1993).
[48]M. Beck, A. Jäckle, G. A. Worth, and H.-D. Meyer, Phys. Rep. **324**, 1 (2000).
[49]H. Guo, J. P. Menzel, and B. Jackson, J. Chem. Phys. **149**, 244704 (2018).
[50]H. Guo and B. Jackson, J. Chem. Phys. **150**, 204703 (2019).
[51]P. Spiering and J. Meyer, J. Phys. Chem. Lett. **9**, 1803 (2018).
[52]B. Jiang, J. Li, and H. Guo, J. Phys. Chem. Lett. **11**, 5120 (2020).
[53]R. Welsch, K. Song, Q. Shi, S. C. Althorpe, and T. F. Miller, J. Chem. Phys. **145**, 204118 (2016).
[54]Q. Liu, L. Zhang, Y. Li, and B. Jiang, J. Phys. Chem. Lett. **10**, 7475 (2019).
[55]H. Jiang, M. Kammler, F. Ding, Y. Dorenkamp, F. R. Manby, A. M. Wodtke, T. F. Miller, A. Kandratsenka, and O. Bünermann, Science **364**, 379 (2019).
[56]J. Behler, Int. J. Quantum Chem. **115**, 1032 (2015).
[57]F. Nattino, C. Díaz, B. Jackson, and G. J. Kroes, Phys. Rev. Lett. **108**, 236104-1 (2012).
[58]B. Jackson, F. Nattino, and G.-J. Kroes, J. Chem. Phys. **141**, 054102 (2014).
[59]G.-J. Kroes, J. I. Juaristi, and M. Alducin, J. Phys. Chem. C **121**, 13617 (2017).
[60]C. Díaz, R. A. Olsen, H. F. Busnengo, and G.-J. Kroes, J. Phys. Chem. C **114**, 11192 (2010).
[61]B. Jiang and H. Guo, Phys. Chem. Chem. Phys. **16**, 24704 (2014).
[62]M. Wijzenbroek, D. M. Klein, B. Smits, M. F. Somers, and G.-J. Kroes, J. Phys. Chem. A **119**, 12146 (2015).
[63]J. L. Chen, X. Y. Zhou, Y. L. Zhang, and B. Jiang, Nat. Commun. **9**, 4039 (2018).
[64]E. W. F. Smeets, J. Voss, and G.-J. Kroes, J. Phys. Chem. A **123**, 5395 (2019).
[65]A. Gonzalez-Lafont, T. N. Truong, and D. G. Truhlar, J. Phys. Chem. **95**, 4618 (1991).
[66]Y.-Y. Chuang, M. L. Radhakrishnan, P. L. Fast, C. J. Cramer, and D. G. Truhlar, J. Phys. Chem. A **103**, 4893 (1999).
[67]S. Mallikarjun Sharada, T. Bligaard, A. C. Luntz, G.-J. Kroes, and J. K. Nørskov, J. Phys. Chem. C **121**, 19807 (2017).
[68]N. Gerrits, E. W. F. Smeets, S. Vuckovic, A. D. Powell, K. Doblhoff-Dier, and G.-J. Kroes, J. Phys. Chem. Lett. **11**, 10552 (2020).
[69]R. Yin, Y. Zhang, F. Libisch, E. A. Carter, H. Guo, and B. Jiang, J. Phys. Chem. Lett. **9**, 3271 (2018).
[70]K. Doblhoff-Dier, J. Meyer, P. E. Hoggan, and G.-J. Kroes, J. Chem. Theory Comput. **13**, 3208 (2017).
[71]A. D. Powell, G.-J. Kroes, and K. Doblhoff-Dier, J. Chem. Phys. **153**, 224701 (2020).
[72]E. W. F. Smeets, G. Füchsel, and G.-J. Kroes, J. Phys. Chem. C **123**, 23049 (2019).
[73]G. Füchsel, K. Cao, S. Er, E. W. F. Smeets, A. W. Kleyn, L. B. F. Juurlink, and G.-J. Kroes, J. Phys. Chem. Lett. **9**, 170 (2018).
[74]Y. Zhang, X. Zhou, and B. Jiang, J. Phys. Chem. Lett. **10**, 1185 (2019).
[75]M. del Cueto, X. Zhou, L. Zhou, Y. Zhang, B. Jiang, and H. Guo, J. Phys. Chem. C **124**, 5174 (2020).
[76]Q. Liu, X. Zhou, L. Zhou, Y. Zhang, X. Luo, H. Guo, and B. Jiang, J. Phys. Chem. C **122**, 1761 (2018).
[77]K. Shakouri, J. Behler, J. Meyer, and G. Kroes, J. Phys. Chem. Lett. **8**, 2131 (2017).
[78]N. Gerrits, K. Shakouri, J. Behler, and G. J. Kroes, J. Phys. Chem. Lett. **10**, 1763 (2019).
[79]T. Liu, B. Fu, and D. H. Zhang, J. Chem. Phys. **151**, 144707 (2019).
[80]H. F. Berger, M. Leisch, A. Winkler, and K. D. Rendulic, Chem. Phys. Lett. **175**, 425 (1990).
[81]S. P. Rittmeyer, V. J. Bukas, and K. Reuter, Adv. Phys.: X **3**, 1381574 (2018).
[82]J. T. Kindt, J. C. Tully, M. Head-Gordon, and M. A. Gomez, J. Chem. Phys. **109**, 3629 (1998).
[83]J. C. Tully, Annu. Rev. Phys. Chem. **51**, 153 (2000).
[84]P. Saalfrank, Chem. Rev. **106**, 4116 (2006).
[85]A. M. Wodtke, D. Matsiev, and D. J. Auerbach, Prog. Surf. Sci. **83**, 167 (2008).
[86]N. Shenvi, S. Roy, and J. C. Tully, Science **326**, 829 (2009).
[87]S. Roy, N. A. Shenvi, and J. C. Tully, J. Chem. Phys. **130**, 174716 (2009).
[88]V. J. Bukas, S. Mitra, J. Meyer, and K. Reuter, J. Chem. Phys. **143**, 034705 (2015).
[89]J. C. Tremblay, J. Chem. Phys. **138**, 244106 (2013).
[90]S. Mandal, T. Sahoo, S. Ghosh, and S. Adhikari, J. Theor. Comput. Chem. **14**, 1550028 (2015).
[91]J. Meyer and K. Reuter, Angew. Chem., Int. Ed. **53**, 4721 (2014).
[92]V. J. Bukas and K. Reuter, Phys. Rev. Lett. **117**, 146101 (2016).
[93]B. Smits and M. F. Somers, J. Chem. Phys. **157**, 134704 (2022).
[94]B. Smits and M. F. Somers, J. Chem. Phys. **158**, 014704 (2023).
[95]M. Dohle, P. Saalfrank, and T. Uzer, Surf. Sci. **409**, 37 (1998).
[96]J. C. Tully, J. Chem. Phys. **73**, 1975 (1980).
[97]S. A. Adelman and J. D. Doll, J. Chem. Phys. **64**, 2375 (1976).
[98]H. F. Busnengo, M. A. Di Césare, W. Dong, and A. Salin, Phys. Rev. B **72**, 125411 (2005).
[99]X. Zhou and B. Jiang, J. Chem. Phys. **150**, 024704 (2019).
[100]B. Jackson and S. Nave, J. Chem. Phys. **138**, 174705 (2013).
[101]S. Nave, A. K. Tiwari, and B. Jackson, J. Phys. Chem. A **118**, 9615 (2014).
[102]V. L. Campbell, N. Chen, H. Guo, B. Jackson, and A. L. Utz, J. Phys. Chem. A **119**, 12434 (2015).
[103]B. Jackson, J. Chem. Phys. **153**, 034704 (2020).
[104]B. Jackson, J. Chem. Phys. **155**, 044705 (2021).
[105]S. Mandal, T. Sahoo, S. Ghosh, and S. Adhikari, Mol. Phys. **113**, 3042 (2015).
[106]J. Dutta, K. Naskar, S. Adhikari, J. Meyer, and M. F. Somers, J. Chem. Phys. **157**, 194112 (2022).
[107]P. Pechukas and J. C. Light, J. Chem. Phys. **44**, 3897 (1966).
[108]G. J. Kroes and M. F. Somers, J. Theor. Comput. Chem. **04**, 493 (2005).
[109]A. Mondal, M. Wijzenbroek, M. Bonfanti, C. Díaz, and G. J. Kroes, J. Phys. Chem. A **117**, 8770 (2013).
[110]A. Togo, L. Chaput, T. Tadano, and I. Tanaka, J. Phys.: Condens. Matter **35**, 353001 (2023).
[111]A. Togo, J. Phys. Soc. Jpn. **92**, 012001 (2023).
[112]B. Smits *et al.* "H_2 on Cu(111) at a surface temperature of 925 K: Effective Hartree potential vs sudden approximation" (unpublished) (2024).